Calculation of Dyson orbitals using a symmetry-adapted-cluster configuration-interaction method for electron momentum spectroscopy: N_2 and H_2O

Y. R. Miao, C. G. Ning,* and J. K. Deng†
Department of Physics, State Key Laboratory of Low-Dimensional Quantum Physics, Tsinghua University, Beijing 100084, People's Republic of China
(Received 7 March 2011; published 15 June 2011)

The symmetry-adapted-cluster (SAC) configuration-interaction (CI) theory was introduced to interpret the non-coplanar symmetric (*e*,2*e*) results. Dyson orbitals derived from the bench-marked SAC CI general-R method were utilized for computing the electron momentum distributions. The corresponding excitation energies and spectroscopic factors can be used to reproduce the ionization spectra. The implementation was demonstrated by examples of N_2 and H_2O. The electron momentum distributions calculated using SAC CI method were compared with recent experimental results, as well as the Hartree-Fock and density-functional-theory calculations. The SAC CI method gave the best performance on the description of the experimental momentum distributions. It was found that the electron momentum distributions of Dyson orbitals related to the satellite lines can be notably different from those of their parent orbitals due to the electron correlation in the initial target states. Present work demonstrated that the SAC CI theory is a very useful and accurate tool for interpreting high-resolution electron momentum spectroscopy results.

DOI: 10.1103/PhysRevA.83.062706 PACS number(s): 34.80.Gs, 31.15.V−

I. INTRODUCTION

Electron momentum spectroscopy (EMS), also called (*e*,2*e*) spectroscopy, is a powerful tool for probing electronic structures of atoms and molecules, as well as the dynamics of electron impact ionizations [1]. A detailed study of the kinetics of the incoming electron and the two outgoing electrons in binary (*e*,2*e*) scattering allows one to measure not only the binding energy spectrum, but also the triple-differential cross section for each peak in the binding energy spectrum. At higher impact energy and higher momentum transfer, this cross section is proportional to the spherically averaged momentum distribution of the related Dyson orbital [1]. Highly accurate Dyson orbitals [2–5] can be obtained from configuration-interaction (CI) [6] or Green's function (GF) calculations [7], which can precisely take into account the electron correlations. Electron correlation is usually defined as the difference between the nonrelativistic exact energy and the Hartree-Fock (HF) energy. The independent particle model always gives the over-estimated electron-electron repulsion. Two different approaches, CI and GF, can be used to remedy the shortcoming. [8–12]. For the outer valence orbitals of molecules, Dyson orbitals can be well approximated using the Hartree-Fock orbital or Kohn-Sham orbital when the electron correlation is not significant [13], but it is not the case for the inner valence orbitals. The frozen orbital approximation cannot account for the existence of satellite lines or for the intensities. In the inner valence region of binding energy spectra, a breakdown of a frozen orbital model happens if electrons are strongly correlated with each other. More powerful theoretical methods such as CI or GF have to be employed in order to obtain agreement with experimental results. In certain molecules, such as H_2O, even the observed momentum distribution of the highest occupied molecular orbital cannot be well described by HF or density-functional theory (DFT) calculations with moderate basis sets [14], but can be interpreted by high level calculations, such as CI or GF [15,16]. It is worth noting that the results of DFT calculations were improved with larger basis sets [13].

Those extra structures, which exist in the inner valence region of binding energy spectra of atoms and molecules, stimulate theorists to develop some high-level many-body theories, such as Green's function method [7,17], and the CI method [6,18]. With the language of CI, the accurate wave functions are described by mixing many configurations. Strong interaction between single-hole configurations and two-hole–one-particle or the higher excitation configurations is the main reason why the extra structures exist in the ionization spectrum. Mixing of these configurations leads to the redistribution of intensities among many states of the same symmetry.

The symmetry-adapted-cluster (SAC) CI method, developed by Nakatsuji [19], is a configuration-interaction method that combines the merits of size consistency of the coupled-cluster theory [20] and the energy upper boundary of the CI theory [10]. And, the symmetry-adapted operators were used to make the calculations more effective.

N_2 and H_2O are two typical molecules which play important roles in quantum chemistry history in both experimental and theoretical aspects [13,15,16,21–24]. In the present work, SAC CI theory was used to calculate the momentum distributions of Dyson orbitals as well as the binding energy spectra of N_2 and H_2O.

II. THEORETICAL BACKGROUND

A. Basic theory of EMS

Electron momentum spectroscopy is based on the kinetically complete (*e*,2*e*) reaction, where high-energy electrons are used as projectiles to ionize atoms or molecules. The scattered electron and the knock-out electron are detected in coincidence. With energy conservation and momentum

*ningcg@tsinghua.edu.cn
†djk-dmp@tsinghua.edu.cn

conservation, the binding energy ε and momentum p of the electron before being knocked out can be given using the kinetics complete experiment:

$$\varepsilon = E_0 - E_f - E_s \quad (1)$$

$$p = p_0 - p_f - p_s \quad (2)$$

The incident and two outgoing electrons are distinguished by subscript $0, f,$ and s, respectively. Our spectrometer takes the non-coplanar symmetric geometry [25]. With this geometry, two outgoing electrons have the same polar angle ($\theta_f = \theta_s = 45^o$) relative to the incident electron beam and the roughly same kinetic energy ($E_f \approx E_s$). The magnitude of the momentum p of the struck electron before the reaction can be determined through the out-of-plane azimuthal angle ϕ:

$$p = \left\{ (2p_f \cos\theta_f - p_0)^2 + \left[2p_f \sin\theta_f \sin\left(\frac{\phi}{2}\right) \right]^2 \right\}^{1/2}. \quad (3)$$

Under the conditions of high momentum transfer and high incident energy, EMS ionization intensities are simply proportional to electronic structure factors obtained as the absolute square of Dyson orbitals in momentum space [1]:

$$\sigma_{\mathrm{EMS}} = \frac{d^5\sigma}{d\Omega_f d\Omega_s dE_f} \propto \frac{1}{4\pi} \int d\Omega \left| \left\langle e^{-ipr} \Psi_i^{N-1} | \Psi_g^N \right\rangle \right|^2. \quad (4)$$

The ground state and the ionized state of the target are represented by ${\Psi_g}^N$ and ${\Psi_i}^{N-1}$, respectively. N is the total electron number. e^{-ipr} is the plane wave. The term $\langle e^{-ipr} \Psi_i^{N-1} | \Psi_g^N \rangle$ presents the Fourier transform of the position-space Dyson orbital, as is called the Dyson orbital in momentum space [1,26]. The integral $\int d\Omega$ represents the spherical average for the randomly oriented molecules in the gas phase. With the target Hartree-Fock approximation or the target Kohn-Sham approximation, Hartree-Fock or Kohn-Sham orbitals can be used to simplify the calculation.

B. SAC method and SAC CI general-R method

The SAC CI method [27–35] is a reliable and powerful tool to study numerous and complicated satellite lines existing in the binding energy spectra of atoms and molecules. To reproduce the fine structures of ionization energy spectra, the electronic correlations in both the ground state and the ionized state need to be accurately calculated. For the single closed-shell state, the ground state is defined by the symmetry-adapted-cluster (SAC) expansion as

$$\left|\Psi_g^{\mathrm{SAC}}\right\rangle = \exp\left(\sum_I C_I S_I\right)|0\rangle = \left(1 + \sum_I C_I S_I + \frac{1}{2}\sum_{I,J} C_I C_J S_I S_J + \cdots\right)|0\rangle, \quad (5)$$

where $|0\rangle$ is the Hartree-Fock ground configuration, S_I is the symmetry-adapted excitation operator, and C_I is the coefficient. The SAC method can greatly simplify the calculation. Furthermore, the SAC method is size consistent because of its nonlinear expansion form [27] while the truncated CI is not [10]. This is a key feature that an ideal molecular orbital (MO) theory should have. The correlated wave functions ${\Psi_e}^{\mathrm{SACCI}}$ of the ionized state are obtained using SAC CI method, which considers electron correlations from the ground state ${\Psi_g}^{\mathrm{SAC}}$:

$$\left|\Psi_e^{\mathrm{SACCI}}\right\rangle = \Re \left|\Psi_g^{\mathrm{SAC}}\right\rangle, \quad (6)$$

Where $\Re$ is an excitation operator. For the multielectron processes, $\Re$ can include up to sextuple excitation operators in the present version of the SAC CI general-R method [27–30]. The Dyson orbital, which is defined as the overlap of the target molecular state and the final ionic state, is given by

$$\Phi_{\mathrm{Dyson}} = \left\langle \Psi_e^{\mathrm{SACCI}} \,\middle|\, \Psi_g^{\mathrm{SAC}} \right\rangle = \sum_j c_j \varphi_j^{\mathrm{HF}}, \quad (7)$$

$$S_g^e = \sum_j c_j^2, \quad (8)$$

where c_j is the coefficient, and ${\phi_j}^{\mathrm{HF}}$ is HF orbital. The norm of the Dyson orbital, S_g^e, called the spectroscopic factor, stands for the probability of the ionization from a particular state. The obtained Dyson orbital is then used to produce the spherically averaged momentum distribution through a Fourier transform [1].

In the present study, the SAC CI method was used to calculate the binding energy spectra and the momentum distributions observed in $(e,2e)$ experiments. Two important molecules N_2 and H_2O were chosen to demonstrate its performance.

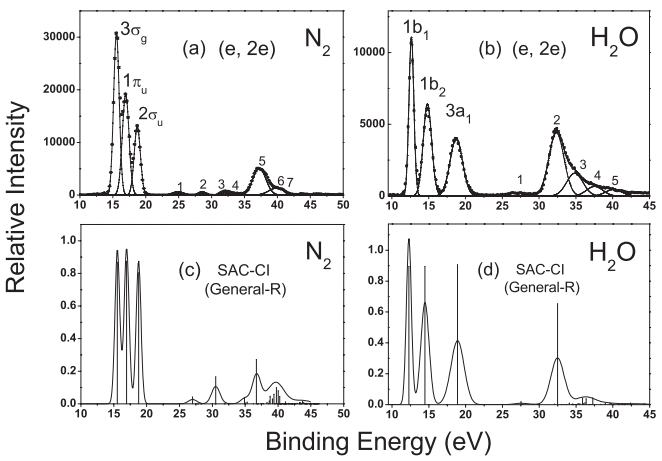

FIG. 1. Comparison of experimental and theoretical binding energy spectra for N_2 and H_2O. (a) $(e,2e)$ experimental binding energy spectrum of N_2 taken from Ref. [40]. (b) $(e,2e)$ experimental binding energy spectrum of H_2O taken from Ref. [16]. (c) Simulated binding energy spectrum for N_2 using the SAC CI general-R method. (d) Simulated binding energy spectrum for H_2O using the SAC CI general-R method. See the text for details.

TABLE I. Ionization potentials (eV), spectroscopic factors (SF), and the Dyson orbitals expanded with HF orbitals for N_2 (most significant three terms according to the magnitude).

	EMS[a]	SAC CI General-R[b] (SF)	Dyson orbital expansion form[c]
$2\Sigma_g^+$			
	15.6(1.00)	15.55(0.871)	$0.932(3\sigma_g)^{-1}+0.026\,(2\sigma_g)^{-1}+0.017(4\sigma_g)^{-1}$
	28.55(0.02)	29.2(0.131)	$-0.338(2\sigma_g)^{-1}+0.122(3\sigma_g)^{-1}-0.020(4\sigma_g)^{-1}$
	32.7(0.01)	35.03(0.027)	$0.144(2\sigma_g)^{-1}-0.078(3\sigma_g)^{-1}+0.006(4\sigma_g)^{-1}$
		35.71(0.197)	$0.437(2\sigma_g)^{-1}-0.077(3\sigma_g)^{-1}+0.004(4\sigma_g)^{-1}$
	37.25(0.4)	36.72(0.272)	$-0.490(2\sigma_g)^{-1}-0.072(3\sigma_g)^{-1}+0.008(4\sigma_g)^{-1}$
		38.41(0.058)	$0.241(2\sigma_g)^{-1}-0.003(4\sigma_g)^{-1}+0.002(3\sigma_g)^{-1}$
	39.9(0.13)	39.77(0.100)	$-0.420(2\sigma_g)^{-1}-0.062(3\sigma_g)^{-1}+0.005(4\sigma_g)^{-1}$
		41.43(0.009)	$-0.091(2\sigma_g)^{-1}+0.008(3\sigma_g)^{-1}-0.006(4\sigma_g)^{-1}$
	43.1(0.03)	41.71(0.014)	$-0.119(2\sigma_g)^{-1}-0.013(3\sigma_g)^{-1}+0.003(4\sigma_g)^{-1}$
		45.30(0.013)	$-0.099(2\sigma_g)^{-1}+0.052(3\sigma_g)^{-1}-0.006(4\sigma_g)^{-1}$
$2\Pi_u$			
	16.95(1.00)	16.96(0.874)	$0.939(1\pi_u)^{-1}+0.006(3\pi_u)^{-1}-0.002(2\pi_u)^{-1}$
$2\Sigma_u^+$			
	18.7(0.80)	18.77(0.802)	$-0.888(2\sigma_u)^{-1}-0.009(3\sigma_u)^{-1}+0.008(4\sigma_u)^{-1}$
	24.9(0.07)	25.53(0.050)	$-0.223(2\sigma_u)^{-1}-0.011(4\sigma_u)^{-1}-0.008(3\sigma_u)^{-1}$
	32(0.04)	33.94(0.049)	$-0.222(2\sigma_u)^{-1}+0.006(4\sigma_u)^{-1}-0.002(3\sigma_u)^{-1}$

[a]Experimental ionization potentials were taken from Ref. [40].
[b]Present work.
[c]Present work.

C. Calculation details for N_2 and H_2O

To proceed with the *ab initio* calculations, the equilibrium experimental geometries were used and the vibrational motion is ignored here; namely, $R_{NN} = 1.098$ Å for N_2 in the $D_{\infty h}$ point groupand $R_{HO} = 0.956$ Å, ∠H—O—H = 105.2° for H_2O in the C_2v point group [32]. The calculations employed the correlated consistent basis set cc-pVTZ [36] augmented with one *s*-type function of $\zeta_s = 0.028$ and one *d*-type function of $\zeta_d = 0.8$ for N [37] and three *s*-type functions of $\zeta_s = 0.059$, $\zeta_s = 0.017$, $\zeta_s = 0.0066$, three *p*-type functions of $\zeta_p = 0.059$, $\zeta_p = 0.015$, $\zeta_p = 0.0054$, and three *d*-type functions of $\zeta_d = 0.059$, $\zeta_d = 0.016$, $\zeta_d = 0.0032$ for O [32], and one *p*-type polarization function of $\zeta_p = 0.8$ for H [38].

In SAC calculation, single excitation operators were included without selection. A double excitation operator was included when its second-order contribution to the energy was larger than a given threshold $\lambda_g = 1.0\times10^{-6}$. Linked operators whose SDCI coefficients larger than 5.0×10^{-3} were included for unlinked terms. In the SAC CI calculation, the perturbation selections were done to reduce the computational time. All single excitation operators were included without selection. Double excitation or higher excitation operators

TABLE II. Ionization potentials (eV), spectroscopic factors (SF), and the Dyson orbitals expanded with HF orbitals for H_2O (most significant three terms according to the magnitude).

	EMS[a]	SAC CI General-R[b] (SF)	Dyson orbital expansion form[c]
$2A_1$			
	14.8(1.00)	14.47 (0.895)	$-0.945(3a_1)^{-1}-0.033(2a_1)^{-1}+0.020(10a_1)^{-1}$
	27.1(0.021)	27.52(0.019)	$0.134(2a_1)^{-1}-0.019(3a_1)^{-1}+0.002(4a_1)^{-1}$
	32.4(0.495)	32.48(0.653)	$0.806(2a_1)^{-1}-0.056(3a_1)^{-1}-0.012(10a_1)^{-1}$
	34.8(0.186)	34.08(0.010)	$-0.090(2a_1)^{-1}-0.044(3a_1)^{-1}-0.004(10a_1)^{-1}$
		35.88(0.042)	$-0.204(2a_1)^{-1}-0.010(10a_1)^{-1}+0.007(3a_1)^{-1}$
		36.38(0.038)	$0.189(2a_1)^{-1}-0.044(3a_1)^{-1}+0.011(9a_1)^{-1}$
	37.5(0.072)	37.27(0.043)	$-0.190(2a_1)^{-1}-0.074(3a_1)^{-1}-0.020(10a_1)^{-1}$
	40.1(0.047)	39.61(0.010)	$0.102(2a_1)^{-1}+0.004(3a_1)^{-1}+0.003(10a_1)^{-1}$
		42.39 (0.010)	$-0.096(2a_1)^{-1}+0.014(3a_1)^{-1}-0.014(9a_1)^{-1}$
$2B_1$			
	12.6(1.00)	12.29(0.895)	$-0.945(1b_1)^{-1}-0.028(4b_1)^{-1}-0.001(3b_1)^{-1}$
$2B_2$			
	18.7(1.00)	18.90(0.906)	$0.952(1b_2)^{-1}+0.013(4b_2)^{-1}+0.006(5b_2)^{-1}$

[a]Experimental ionization potentials were taken from Ref. [16].
[b]Present work.
[c]Present work.

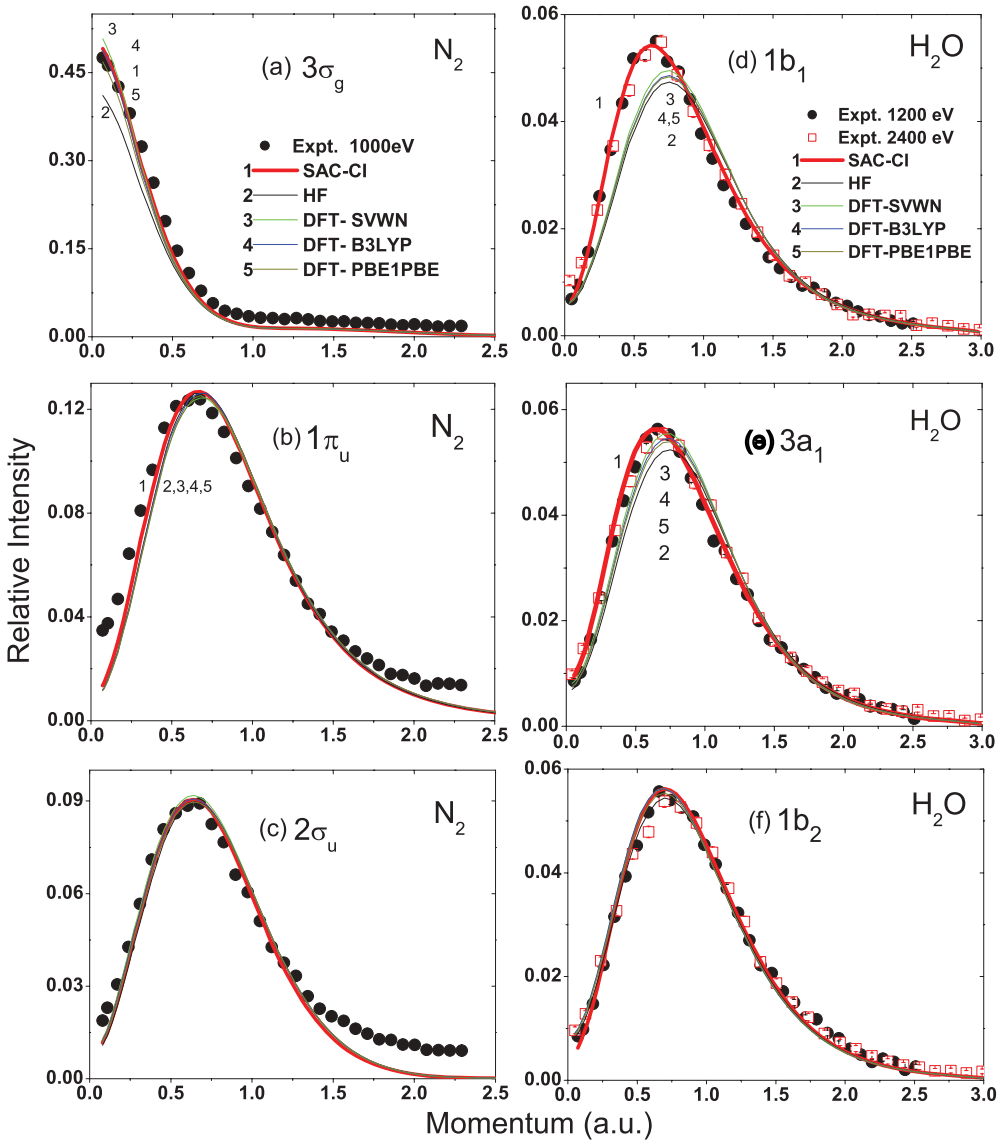

FIG. 2. (Color online) Comparisons of SAC CI, HF, and DFT predictions of three outer valence orbitals momentum distributions with experimental ones for N_2 and H_2O. Experimental data are taken from Refs. [40] and [16].

which satisfied $\lambda_e = 1.0\times10^{-7}$ were selected in the calculation. For unlinked terms we chose all the double excitation operators which satisfied $\tau_e = 0.05$ [27,30,33].

Since N_2 belongs to the $D_{\infty h}$ point group, which has degenerate π orbitals, SAC CI calculations were performed in its nondegenerated subgroup D_{2h}.

The ionization spectra of N_2 and H_2O were calculated by the SAC CI general-R method in both inner and outer valence regions. Target and ion wave functions were expanded in terms of configurations constructed from the ground Hartree-Fock orbitals which served as a basis for the interpretation of the electron correlations. The SAC CI calculations in the present work were performed using the GAUSSIAN03 program [39]. The obtained Dyson orbital, the full target-ion overlapping of the converged SAC ground-state wave function and the SAC CI excited state wave function, was then used to calculate the spherically averaged momentum distribution with our NEMS program [16]. To compare with the experimental momentum distribution, the calculated distribution has been convoluted with the experimental resolution [16].

III. RESULTS AND DISCUSSION

A. Binding energy spectra of N_2 and H_2O

Figure 1 compares the EMS experimental binding energy spectrum (BES) [16,40] with the SAC CI-simulated BES for N_2 and H_2O. The labels of peaks in the outer valence region (<20 eV) are the orbital assignment, and the numbers for peaks in the inner valence region (>20 eV) represents the numbering of Gaussian peaks used for fitting. The spikes in Figs. 1(c) and 1(d) represent the ionization potentials and the spectroscopic factors of the corresponding Dyson orbitals calculated using the SAC CI method. Those spikes were then convolved with a series of Gaussian functions, whose areas are equal to the theoretical spectroscopic factors, and whose widths are equal to the combination of the peak widths from the high-resolution photoelectron spectroscopy and the

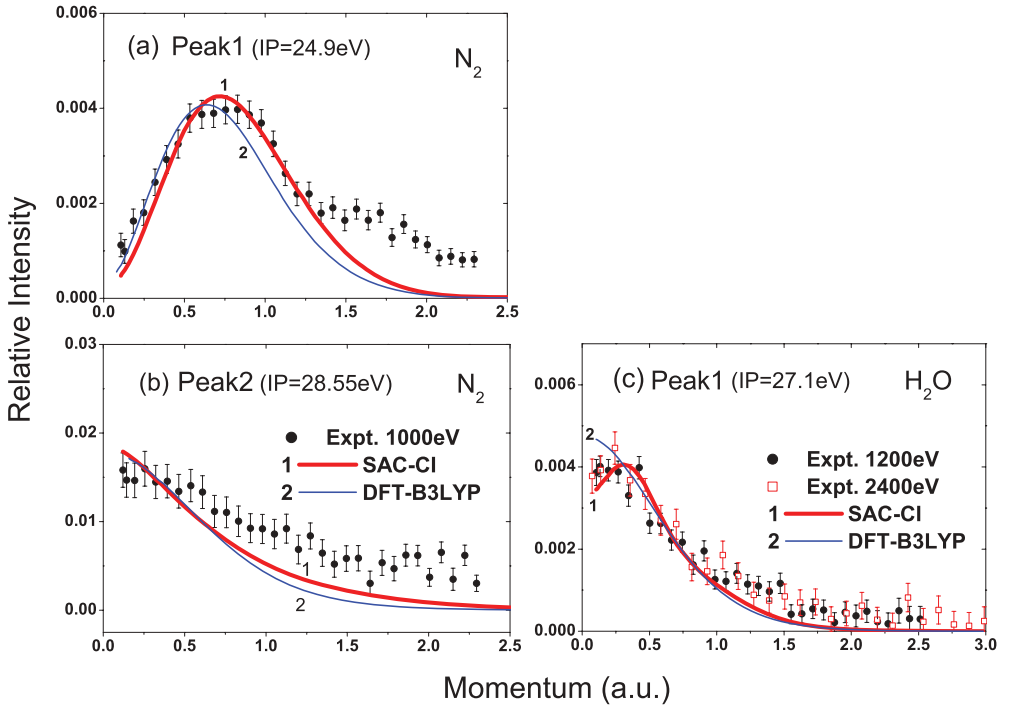

FIG. 3. (Color online) Momentum distributions of three well resolved Dyson orbitals in the inner valence region of N_2 and H_2O. Experimental data were taken from Refs. [40] and [16]

$(e,2e)$ instrumental energy resolution. It can be seen that SAC CI theory can well reproduce the structures of experimental BES. The detailed ionization potentials of N_2 and H_2O are summarized in Tables I and II.

For N_2, the SAC CI calculation predicted three mainlines at 15.55, 16.96, and 18.77 eV, which corresponds to the $(3\sigma_g)^{-1}$, $(1\pi_u)^{-1}$, $(2\sigma_u)^{-1}$ one-hole states. For H_2O, the calculation predicted 12.3 eV $[(1b_1)^{-1}]$, 14.5 eV $[(3a_1)^{-1}]$, and 18.9 eV $[(1b_2)^{-1}]$ mainlines. These predictions are in excellent agreement with the experimental results. From Tables I and II, it can be seen that these sharp peaks are mainly produced by the one-hole configurations in the final state of the N_2 or H_2O molecules, which means that the independent particle model is still a good approximation for these outer valence orbitals. But for the inner valence orbitals, the orbital picture is no longer valid. As indicated by SAC CI calculations and experimental BES, there are many satellite lines in the higher binding energy region (>20 eV) due to the breakdown of molecular orbitals. To obtain the momentum distributions for these satellite lines, seven Gaussian peaks were used to fit the experimental BES in the region for N_2, and five for H_2O.

As Tables I and II indicate, the inner valence one-hole state $(2\sigma_g)^{-1}$ of N_2 and $(3a_1)^{-1}$ of H_2O exhibited much smaller spectroscopic factors, which was due to the severe redistribution of intensities among many multiple-excitation states. Therefore, the independent particle model was no longer valid. The fine interpretation of the observed results must resort to the high level many-body theories, such as the SAC CI, to construct Dyson orbitals. The linear combination of HF orbitals for these Dyson orbitals are also summarized in Tables I and II.

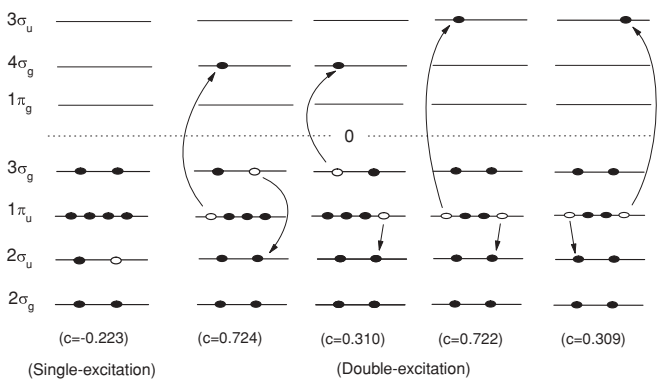

FIG. 4. One-up and one-down mechanism for Dyson orbitals at 24.9 eV of N_2.

B. Momentum distributions of outer valence orbitals for N_2 and H_2O

Experimental profiles for three outer valence orbitals of N_2 were compared with the spherically averaged electron momentum distributions calculated by SAC CI, DFT, and HF with the correlated consistent basis set cc-pVTZ in Figs. 2(a)–2(c). All calculations can well reproduce the experimental momentum distributions. For the $3\sigma_g$ orbital [Fig. 2(a)], there is no discernable difference between the SAC CI and DFT approaches. Both are in excellent agreement with observed results. However, the HF calculation underestimates intensity at the low-momentum region $p < 0.5$ a.u., which reflects that the electron correlation is important for accurately describing this orbital. For $1\pi_u$ and $2\sigma_u$ orbital, the SAC CI, HF, and DFT calculations produced almost the same distributions. The discrepancy between experimental results and calculations

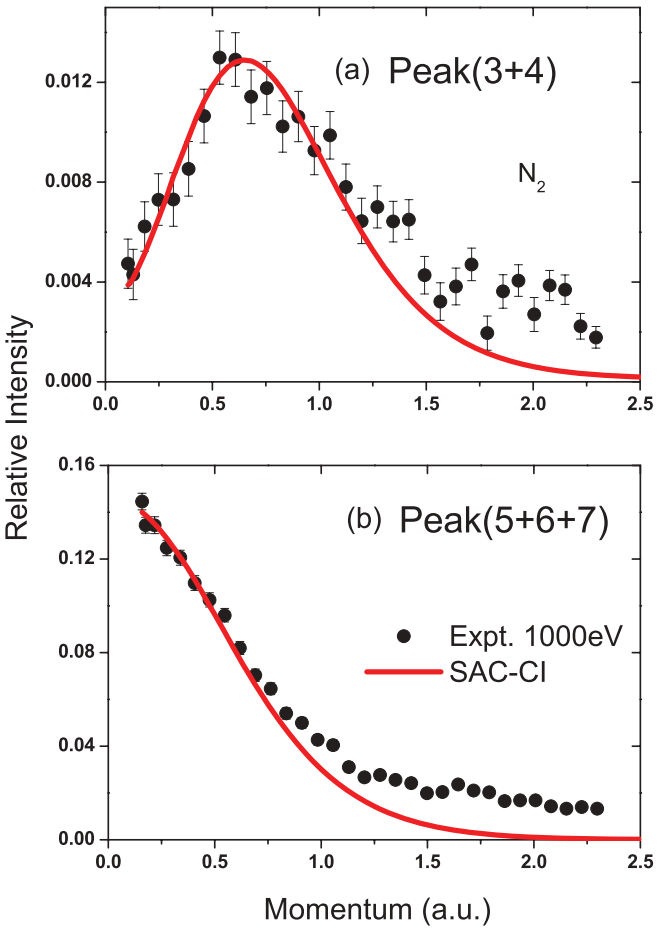

FIG. 5. (Color online) Momentum distributions of summed satellite lines in the inner valence region of N_2. Experimental data were taken from Ref. [40].

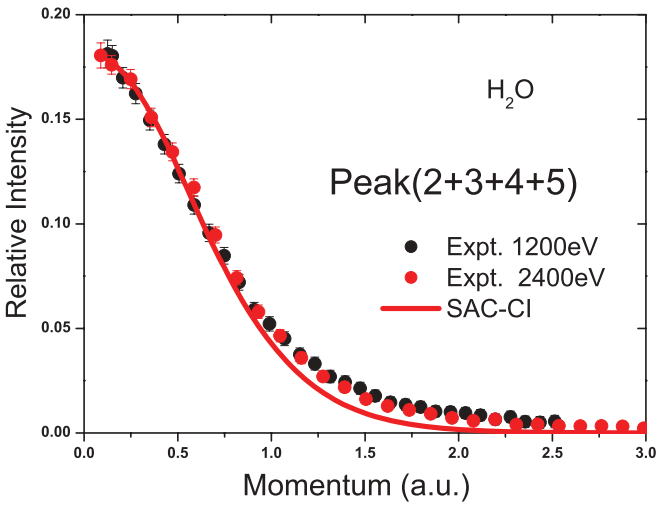

FIG. 6. (Color online) Momentum distributions of summed satellite lines in the inner valence region of H_2O. Experimental data were taken from Ref. [16].

in the high-momentum region ($p > 1.5$ a.u.) in Fig. 2(c) may be the result of the distorted-wave effects [41]. The electron with a higher momentum is closer to the nuclei, so the Coulomb potential influences the continuum electrons more. As a result, the plane wave cannot fully represent the incoming and outgoing electrons. The performances of HF and DFT are almost the same as SAC CI, which indicated that the independent particle model is still pretty good for outer valence orbitals of N_2.

Momentum distributions of outer valence orbitals of H_2O have been extensively investigated by experiments and theories [13,15,16,21]. As shown in Figs. 2(d) and 2(e), with the same correlated consistent basis set cc-pVTZ, our high-level SAC CI calculation agrees with the experimental results much better than HF and DFT, which demonstrated again the importance of the electron correlation for accurately describing the experimental momentum distributions.

C. Momentum distributions of three well-resolved inner valence Dyson orbitals for N_2 and H_2O

There are two experimentally well-resolved Dyson orbitals of N_2, which are located at 24.9 and 28.55 eV, respectively [peaks 1 and 2 in Fig. 1(a)]. As shown in Figs. 3(a) and 3(b), our SAC CI calculations can well reproduce their experimental momentum distributions. Since the independent particle model is not valid for these peaks, only the SAC CI method can directly provide an interpretation of these results. If the electron correlation of the initial state is not significant, the momentum distribution of the satellite line is very close to that of its parent orbital. This is the reason why the momentum distributions of parent orbitals multiplied by the spectroscopic factors are widely used for explaining momentum distributions of satellite lines, when direct calculations for satellite lines are not available. In Fig. 3, DFT calculations were also plotted in comparison with experimental results. It is obvious that SAC CI calculations presented a better description of experimental distributions than the DFT ones.

The Dyson orbital at 27.1 eV of H_2O [16] [peak 1 in Fig. 1(b)] is one typical example given to emphasize the significance of electron correlations in the initial state. As shown in Fig. 3(c), the SAC CI method excellently reproduced the experimental momentum distributions, but the DFT approach overestimated the experimental intensity in the $p < 0.5$ a.u. region. The DFT calculated distributions, which were estimated from its parent orbital, are quite different from of the SAC CI results. The DFT approach predicted a maximum intensity at the momentum origin, and it monotonously decreases as p increases. However, SAC CI calculations predicted a local minimum intensity at the momentum origin. As p increases, it first increases and gets its maximum at $p = 0.4$ a.u., then decreases. The calculated overall shape matched the experimental profile very well. It is interesting to note that the third-order algebraic diagrammatic construction scheme (ADC(3)) method cannot reproduce the experimental results for this satellite line [16].

According to the SAC CI calculation, the virtual orbitals $4\sigma_u$ and $3\sigma_u$ play an important role in the Dyson orbital at 24.9 eV due to electron correlations in the ground state. An important mechanism called one-up and one-down [42], which leads to the final state of the Dyson orbital at 24.9 eV, is shown in Fig. 4. Final-state correlations are also important to interpret

the satellite because coefficients of these configurations are substantial.

D. Momentum distributions of other inner valence Dyson orbitals for N_2 and H_2O

Peaks 3, 4, 5, 6, and 7 in the inner valence region of N_2 were not well resolved in $(e,2e)$ experiments, as illustrated in Fig. 1(a). In order to make the comparison more reliable and reasonable, peaks were summed up in two groups, peaks (3 + 4) and peaks (5 + 6 + 7), for comparing with the SAC CI calculations in Fig. 5.

Peaks (3 + 4) in Fig. 5(a) exhibit a *p*-type distribution and peaks (5 + 6 + 7) in Fig. 5(b) exhibit an *s*-type distribution. The main sources of these peaks are shown in Table I. As shown in Fig. 5, the SAC CI method can reproduce the experimental momentum distributions.

Peaks in the inner valence region of water from 30 to 40 eV in Fig. 1(b) are summed up and compared to the SAC CI prediction in Fig. 6. The calculated profile is also in good agreement with the experimental momentum profile. The discrepancies in the high-momentum region in Figs. 3, 5, and 6 are very likely still due to the distorted-wave effect [41] because electrons from the inner valence region have more chances to appear near the nuclei than those from the outer valence region.

IV. SUMMARY

The spherically averaged momentum distributions of Dyson orbitals and binding energy spectra of N_2 and H_2O have been calculated using the SAC CI method. Dyson orbitals were calculated through the full overlaps of converged SAC ground-state wave functions and SAC CI excited wave functions. Theoretical momentum distributions calculated using the SAC CI method were compared with HF and DFT calculations, as well as the experimental results. The SAC CI method can excellently reproduce the EMS experimental results for both the momentum distributions and binding energy spectra. It was found that electron correlations in the ground state play an important role in describing the momentum distributions, which was clearly shown with the results of the satellite line at 27.1 eV of H_2O. This work demonstrated that the SAC CI method is a powerful tool for interpreting the high-resolution EMS results.

ACKNOWLEDGMENTS

This work was supported by the National Nature Science Foundation of China under Contracts No. 11074144, No. 10874097, and No. 10704046 and by the Specialized Research Fund for the Doctoral Program of Higher Education under Grant No. 20070003146.

[1] E. Weigold and I. E. McCarthy, *Electron Momentum Spectroscopy* (Kluwer/Plenum, New York, 1999).
[2] R. K. Singh, J. V. Ortiz, and M. K. Mishra, Int. J. Quantum Chem. **110**, 1901 (2010).
[3] C. M. Oana and A. I. Krylov, J. Chem. Phys. **127**, 234106 (2007).
[4] M. Yamazaki, T. Horio, N. Kishimoto, and K. Ohno, Phys. Rev. A **75**, 032721 (2007).
[5] M. E. Casida and D. P. Chong, Int. J. Quantum Chem. **40**, 225 (1991).
[6] R. L. Martin and D. A. Shirley, Phys. Rev. A **13**, 1475 (1976).
[7] W. Von Niessen, J. Schirmer, and L. S. Cederbaum, Comp. Phys. Rep. **1**, 57 (1984).
[8] R. J. Bartlett, Chem. Phys. Lett. **484**, 1 (2009).
[9] J. A. Pople, R. Seeger, and R. Krishnan, Int. J. Quantum Chem. **11**, 149 (1977).
[10] J. A. Pople, R. Krishnan, H. B. Schlegel, and J. S. Binkley, Int. J. Quantum Chem. **14**, 545 (1978).
[11] R. L. Martin and D. A. Shirley, J. Chem. Phys. **64**, 3685 (1976).
[12] E. Weigold, I. E. McCarthy, A. J. Dixson, and S. Dey, Chem. Phys. Lett. **47**, 209 (1977).
[13] P. Duffy, D. P. Chong, M. E. Casida, and D. R. Salahub, Phys. Rev. A **50**, 4707 (1994).
[14] A. O. Bawagan, L. Y. Lee, K. T. Leung, and C. E. Brion, Chem. Phys. **99**, 367 (1985).
[15] A. O. Bawagan, C. E. Brion, E. R. Davidson, and D. Feller, Chem. Phys. **113**, 19 (1987).
[16] C. G. Ning *et al.*, Chem. Phys. **343**, 19 (2008).
[17] C. G. Ning *et al.*, Chem. Phys. Lett. **421**, 52 (2006).
[18] J. Rolke, Y. Zheng, C. E. Brion, Z. Shi, S. Wolfe, and E. R. Davidson, Chem. Phys. **244**, 1 (1999).
[19] H. Nakatsuji and K. Hirao, Chem. Phys. Lett. **59**, 362 (1978).
[20] R. J. Bartlett and M. Musial, Rev. Mod. Phys. **79**, 291 (2007).
[21] A. J. Dixon, S. Dey, I. E. McCarthy, E. Weigold, and G. Williams, Chem. Phys. **21**, 81 (1977).
[22] S. T. Hood, A. Hamnett, and C. E. Brion, J. Electron Spectrosc. Relat. Phenom. **11**, 205 (1977).
[23] R. Cambi, G. Ciullo, A. Sgamellotti, C. E. Brion, J. P. D. Cook, I. E. McCarthy, and E. Weigold, Chem. Phys. **91**, 373 (1984).
[24] R. Cambi, G. Ciullo, A. Sgamellotti, C. E. Brion, J. P. D. Cook, I. E. McCarthy, and E. Weigold, Chem. Phys. **98**, 166 (1985).
[25] C. G. Ning *et al.*, Chin. Phys. B **17**, 1729 (2008).
[26] R. J. F. Nicholson, I. E. McCarthy, and W. Weyrich, J. Phys. B **32**, 3873 (1999).
[27] H. Nakatsuji, J. Chem. Phys. **83**, 5743 (1985).
[28] H. Nakatsuji, J. Chem. Phys. **94**, 6716 (1991).
[29] H. Nakatsuji, Chem. Phys. Lett. **177**, 331 (1990).
[30] H. Nakatsuji, Chem. Phys. **75**, 425 (1983).
[31] H. Nakatsuji, J. Chem. Phys. **113**, 2949 (2000).
[32] M. Ehara, M. Ishida, and H. Nakatsuji, J. Chem. Phys. **114**, 8990 (2001).
[33] H. Nakatsuji, Chem. Phys. Lett. **177**, 331 (1991).
[34] M. Ehara, Y. Ohtsuka, H. Nakatsuji, M. Takahashi, and Y. Udagawa, J. Chem. Phys. **122**, 234319 (2005).
[35] M. Ehara, M. Ishida, and H. Nakatsuji, J. Chem. Phys. **117**, 3248 (2002).
[36] T. H. Dunning, J. Chem. Phys. **90**, 1007 (1989).
[37] M. Ehara and H. Nakatsuji, Chem. Phys. Lett. **282**, 347 (1998).
[38] M. Ehara, S. Yasuda, and H. Nakatsuji, Z. Phys. Chem. **217**, 161 (2003).
[39] M. J. Frish *et al.*, *Gaussian 03* (Gaussian Inc., Pittsburgh, PA, 2003).
[40] S. F. Zhang *et al.*, Acta Phys. Sin. **58**, 2382 (2009).
[41] I. E. McCarthy and E. Weigold, Rep. Prog. Phys. **54**, 789 (1991).
[42] R. L. Martin and E. R. Davidson, Chem. Phys. Lett. **51**, 237 (1977).